XMM/EPIC MOS FM1 & FM2 Ground Calibration at Orsay

Description of product release v1.2

Philippe Marty, Bernard Jean-Philippe
Institut d'Astrophysique Spatiale
Université Paris XII, Bat 121
91405 Orsay Cedex, France.

1 Description of Orsay MOS3 & MOS2 calibration product v1.2

This document shortly describes the content of the calibration files delivered to ESA for the XMM/EPIC MOS camera Flight Model 1 (a.k.a. Orsay-MOS3)

- released on March, 31st 2000, from software v1.2;
- previous releases:
  - October, 8th 1999, from software v1.0 (profiles were not corrected for "stretch effects" leading to QE values 0.01% to 27.52% different from current values and greater error bars than current; error bars were expressed in percent of the corresponding QE value rather than in QE units).
  - March, 10th 2000, from software v1.1 (some runs were still logged at the wrong energy leading to misplaced and/or miscomputed QE points).

and Flight Model 2 (a.k.a. Orsay-MOS2).

- released on March, 31st 2000, from software v1.2;
- previous releases:
  - none.

This delivery includes the following fits files:

- MOS2_QE_v1.2.fits
- MOS3_QE_v1.2.fits

which contains the quantum efficiency (see Fig. 1) for respectively the MOS Orsay2 & MOS Orsay3 cameras. The way these values were derived from the calibration in Orsay is described in the following sections.

2 Calibration Data Taking Strategy

2.1 General Description

The calibration of MOS2 camera was performed in the calibration facility at IAS in March and April 1998, MOS3 in July 1998. We used the 2 synchrotron beam lines (SACO: E $<$ 1.3keV and DCI:1.5 $<$ E $<$ 15keV) shown schematically on Fig. 3. On each beam line, a set of cutoff mirrors and a monochromator (using Bragg crystals on DCI and gratings on SACO) is used to

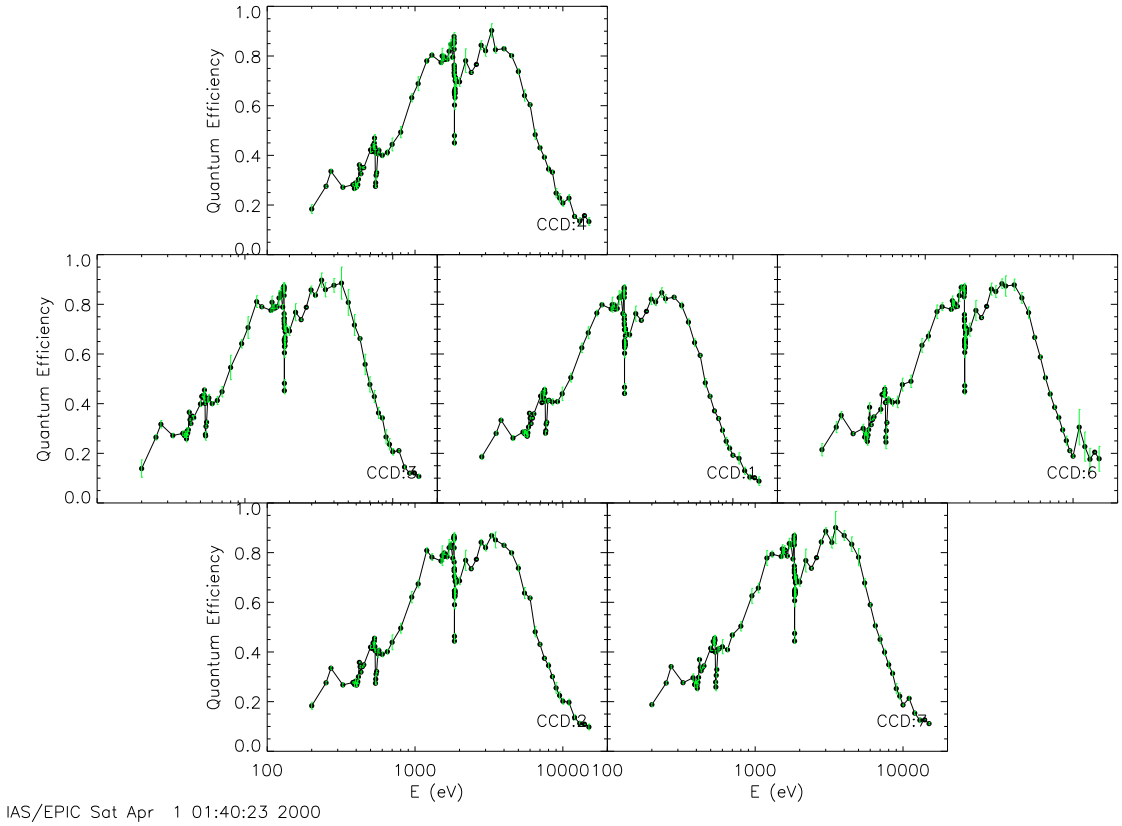

Figure 1: Quantum Efficiency of each CCD of MOS Orsay2.

select the requested energy (spectral purity better than 1%). The camera to be calibrated is located into a vaccuum chamber (Jupiter tank) and can be directed alternatively toward one beam line or the other. A resizing slit is located in front of the camera in the Jupiter tank and is used to select a thin horizontal slice of the beam, as homogeneous as possible, which is sent to the camera. The camera can then move behind the slit in the vertical direction under control of the MOGSE (Mechanical Optical Gound Support Equipment). All devices, except EPIC instrument itself, are remote controlled by a computer network running a shared software designed on purpose, known as the EICC, and capable of sending commands, reading housekeeping data (i.e. device monitorings and data, except EPIC data) and storing them in a file database.

Typically 2 types of calibration runs were performed:

- QE measurement runs consisting of measurements with the OPEN position of the camera filter wheel interleaved with absolute measurements of the beam (typically OPEN, absolute, OPEN)
- QE and Filter transmission runs consisting of measurements with the OPEN position of the camera filter wheel before and after a series of absolute measurement of the beam and camera measurements through the various camera filters (typically OPEN, absolute, A THIN, B THIN, C MEDIUM, D THICK, OPEN)

2.2 Camera operating mode

The MOS camera is read at the end of each vertical scan, also called MOGSE frame, while the camera is no longer illuminated. The MOGSE movements were synchronized so that another

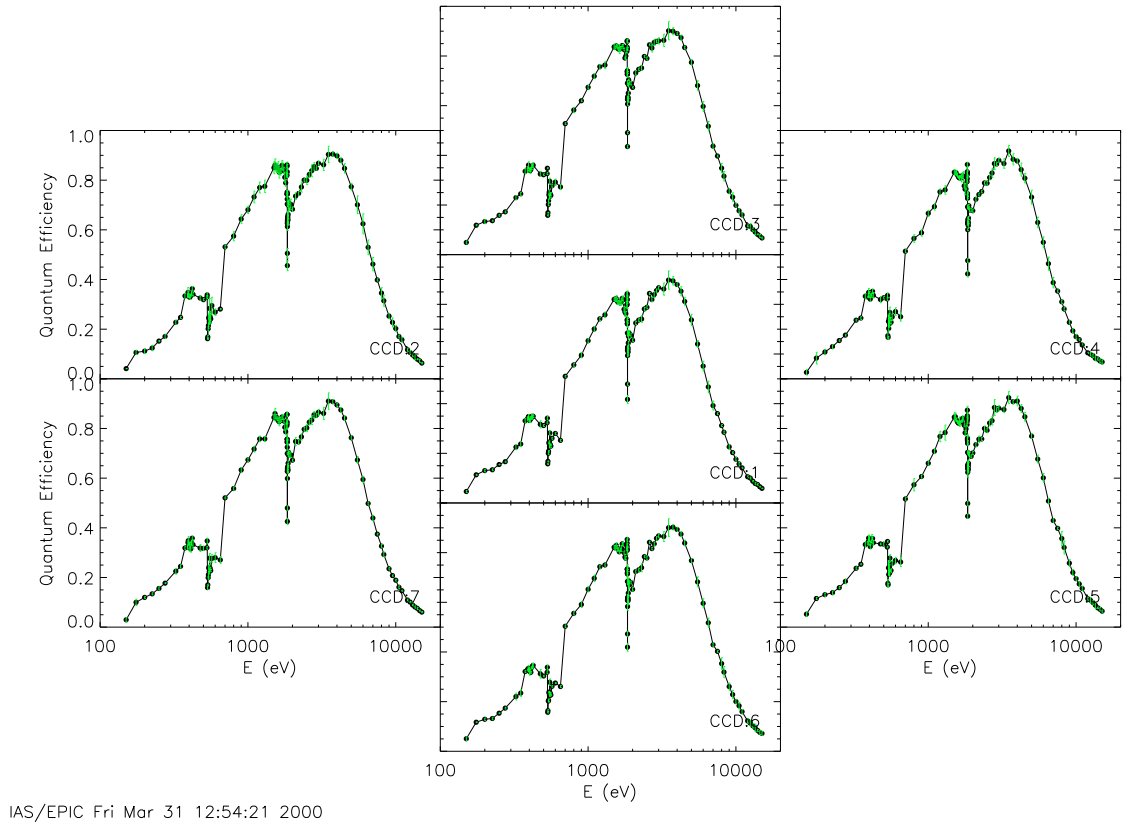

Figure 2: Quantum Efficiency of each CCD of MOS Orsay3.

scan couldn't begin before the camera read-out was completed.

All data were obtained in the full frame imagery mode of the camera, with a threshold of in general 25 ADU for all 7 CCDs for MOS3 and 35 EDU for all 6 CCDs (there was no CCD #5) for MOS2. Resulting QE values were derived from all-patterns events.

It is to be reminded that among MOS2 CCDs we did calibrate in Orsay only CCDs #1,2,6 and 7 are currently flying on XMM satellite. In addition, these flying CCDs aren't located the same way any longer (e.g. CCD #1 at Orsay is not the flying central CCD, but has been relocated at one edge; please refer MOS-Leicester technical documentation).

2.3 Beam calibration

The beam calibration during the MOS2 & MOS3 campaign was performed using a Si(Li) and a Gaz Proportional Counter (GPC) detector.

The Si(Li) detector was calibrated in absolute at Bessy using a white synchrotron beam with no optics. The resulting quantum efficiency of the Si(Li) detector is shown in Fig. 4.

The GPC detector was designed and calibrated at Orsay relatively to the Si(Li) detector. The resulting quantum efficiency of the GPC detector is shown in Fig. 5.

After setting a given beam line to the requested energy, an horizontal profile of the beam is obtained by scanning one of the absolute detector behind the resizing slit. These profiles are used to monitor the shape of the beam along the horizontal axis and to derive the absolute flux at the given energy.

The absolute detector counts at each position are recorded along with the detector position on the horizontal axis (CSY) in the EICC files. The file also contains information about fixed settings of the beam line, such as the integration time used for the measurements.

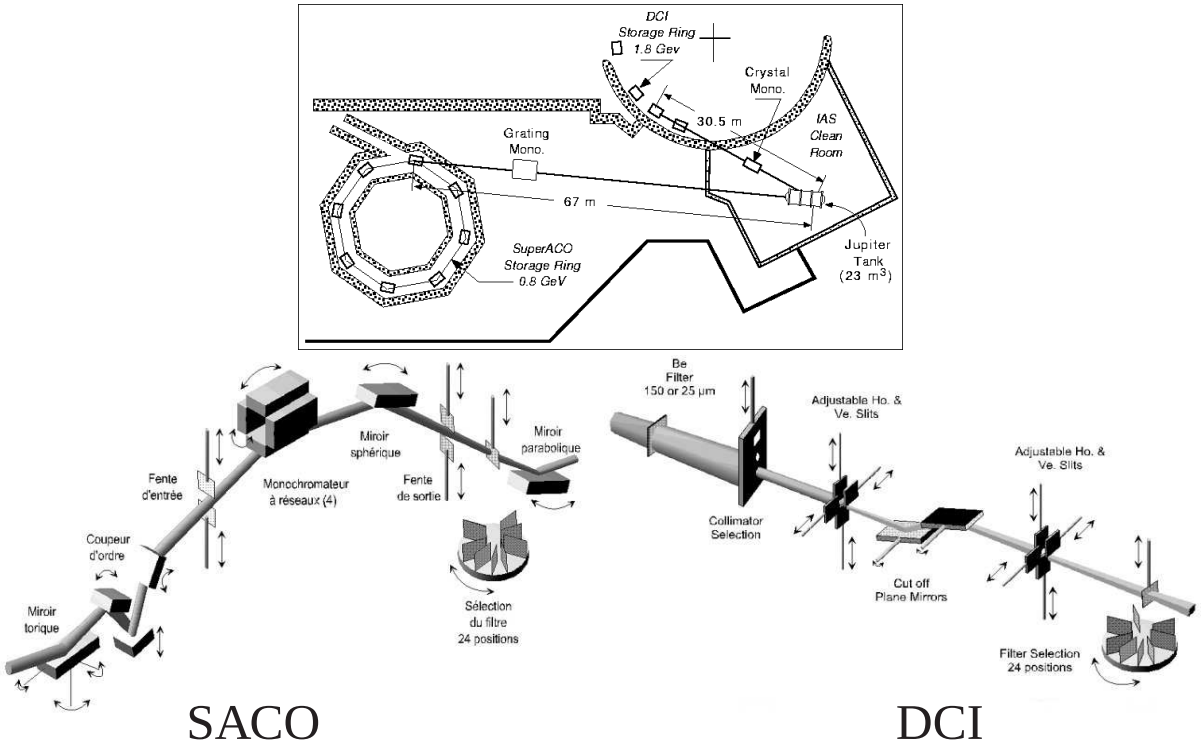

Figure 3: Schematic view of the two beam lines used.

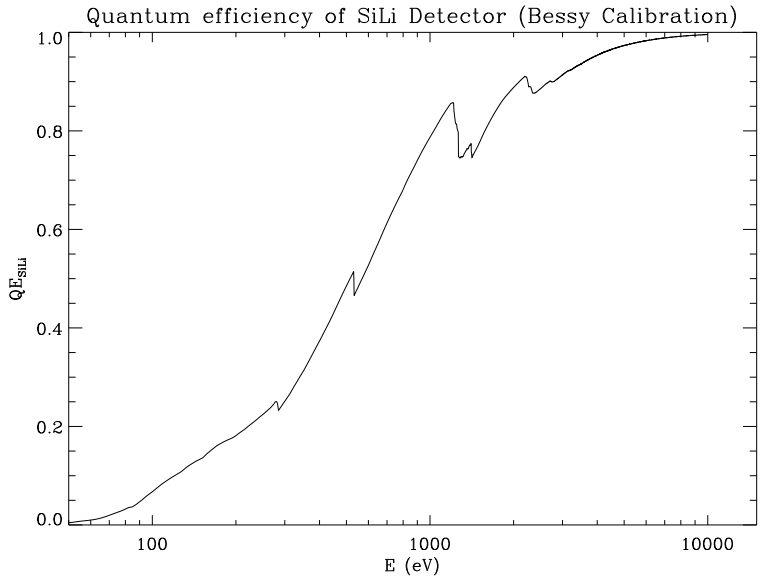

Figure 4: Quantum efficiency of the Si(Li) detector from Bessy measurements.

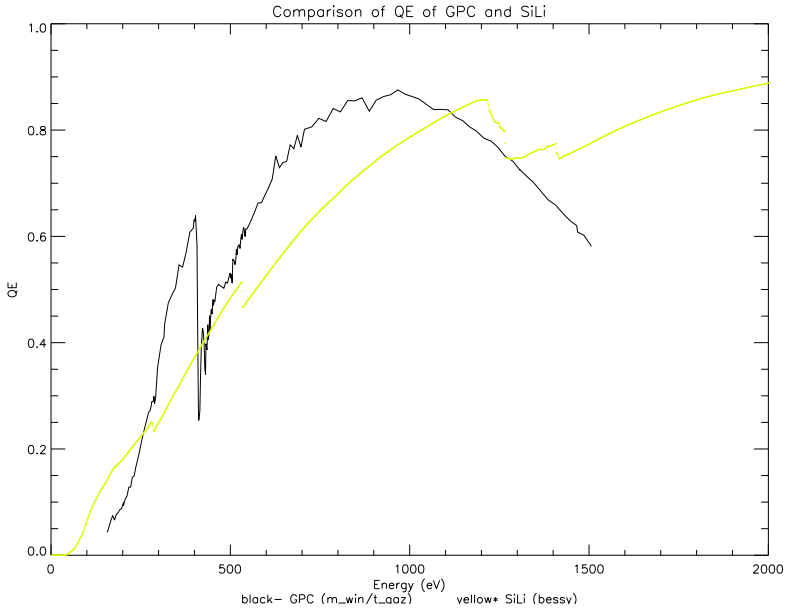

Figure 5: Quantum efficiency of the GPC detector from Orsay measurements. Yellow curve is the Si(Li) QE curve for comparison.

The absolute detector counts are integrated over the spectrum recorded by the detector within 4 Region Of Interest (ROI) in energy. For the Si(Li) detector, the ROIs were the same as those used during the absolute calibrations of the detector at Bessy. The full spectra are not stored for every CSY point along the profile, but the average spectrum over the beam profile is recorded for each run.

2.4 Monitorings

Since the camera data and the absolute measurements cannot be measured at the same time, it is necessary to monitor the evolution of the beam intensity during data acquisition. Three types of continuous monitorings, located at various locations along the beam lines, were used during the MOS calibrations:

- **Synchrotron Current:** The values of the synchrotron current read from SACO and DCI are continuously recorded.
- **Monochromator Diode:** A diode measures the intensity of orders rejected by the monochromator at the level of the monochromator device.
- **Chaneltron measurements:** The beam flux is measured at the level of the entrance slit in the Jupiter Tank with a channeltron detector.

All monitoring data are stored constantly into files through the EICC network and are stamped using a unique time reference, which allows post-synchronization with the data.

2.5 Comb alignment between beam profiles and the EPIC CCDs

The alignement between beam profiles and the EPIC CCDs has been measured by inserting a comb in the synchrotron beam in front of the resizing device and obtaining a beam profile with the Si(Li) detector, then an image with the camera using both beam lines. The comparison of

the positions of the shadow regions on the camera and the absolute profile allows to calibrate the position offset between the CSY axis of the absolute profiles and the pixels of the CCD.

3 Processing applied to calibration data

3.1 Overall data reduction strategy

The overall data reduction strategy is summarized within Fig. 6. First, the log files (both digital and handwritten) are used to generate simple ascii files which can be used to describe what runs have been obtained and contain useful information. The EICC files which were obtained during calibrations are reprocessed into more handy data structures (so called beam structures) in which only the useful information is kept. For a given series of runs obtained at the same energy, the following tasks are performed:

- Extract all parameters relevant to the selected runs in the calibration EICC database (e.g. requested energy, beam line used, vertical position of the camera, absolute beam profile and spectrum, quantum efficiency of the absolute detector interpolated at the energy of the runs...
- Deglitch the absolute beam profile. This is done by running a glitch filter routine over a horizontal profile build on the ROI4 signal, which contains very little real signal; and then removing the points in the all-ROIs profile corresponding to glitches found for ROI4. In case of several integrations at each profile position, these values are finally averaged.
- Fit the absolute spectrum using a hypermet curve in order to derive the energy of the peak and thus check the energy of the beam (consistency with logbook).
- Extract a continuous stream of monitoring data over the time range covered by the absolute and camera data taking.
- Save a beam structure on disk.

Then, these beam structures are compared to similar datasets describing the camera measurements, which were prepared by the Saclay team. The goal of this comparison is to check whether the various beam monitorings give an accurate description of the behavior of the beam during the camera and the absolute measurement data. For a given series of runs obtained at the same energy, the following tasks are performed:

- Check the availability of monitorings during each camera run of the series and during the absolute measurements. For each run and monitoring, a flag containing the percentage of monitoring availability is computed.
- Detect possible sudden jumps of each monitorings, either during camera data taking, absolute beam calibration, or in between. A series of flags containing the date and intensities of the jumps is generated.
- Generate a plot of each monitoring behavior over the considered time range, and overplot the signal from the camera, as well as the difference between back and forth absolute beam profile measurements (see Fig. 7).
- Select the best monitoring : For each monitoring, we compute the average relative difference between the signal as seen by the the camera in the OPEN filter positions and the monitoring signal. This value is used as a flag giving the goodness of each monitoring. However, the reliability of this flag is not high enough, and eye inspection of the plots was generally necessary in order to derive the best monitoring to be used for each series.

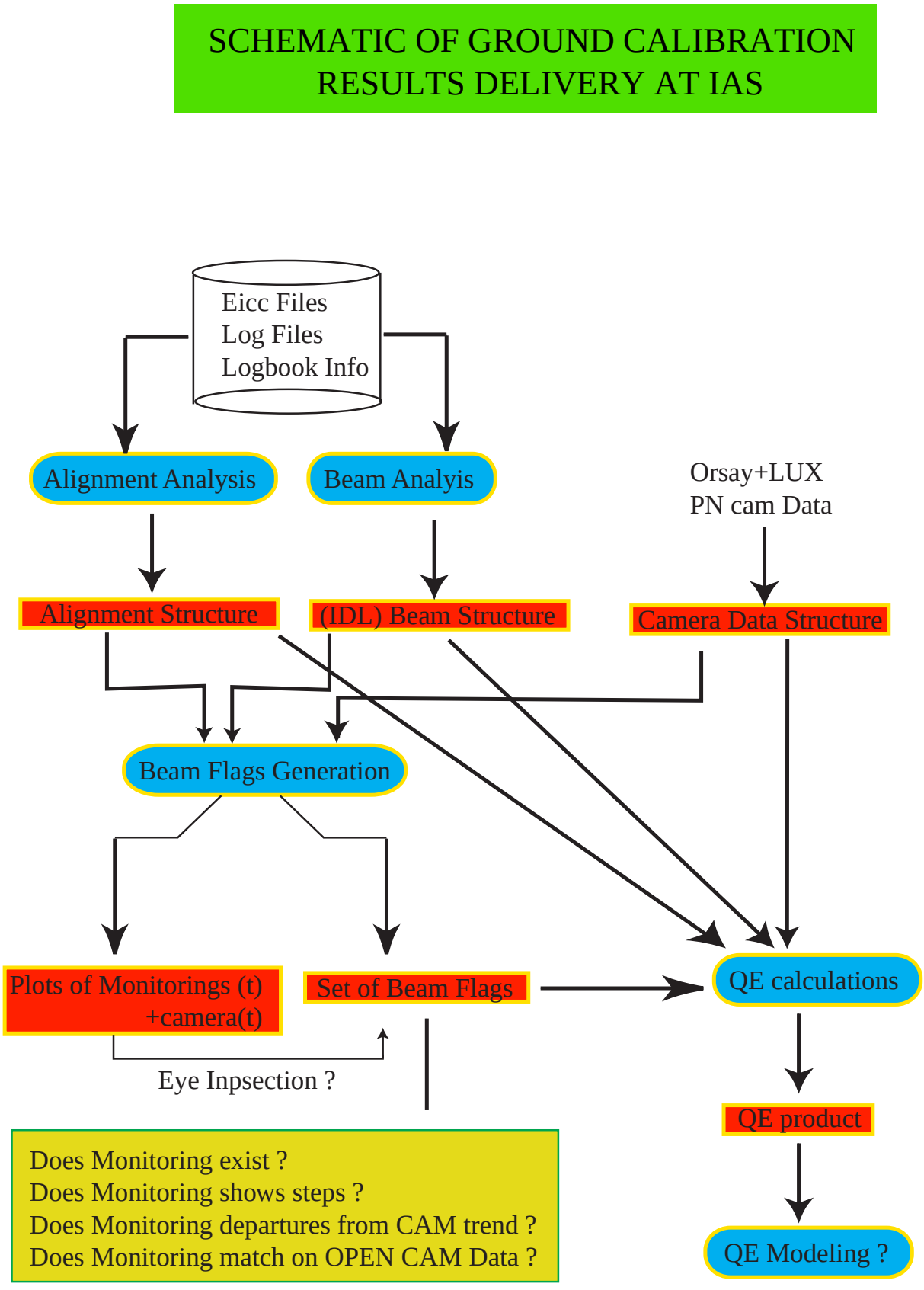

Figure 6: Overall data processing strategy.

- In several occasions, it was found that none of the monitorings adequately represents the behaviour of the signal seen by the camera in the OPEN position, but that a linear correction on one of the monitorings would better reproduce the camera trend. Since this occurs in general with the monochromator monitoring for runs where the synchrotron current is linearly drifting, this effect is currently being interpreted as a superposition of both (but that has not been verified on a systematic basis). In such cases, a linear correction is thus applied to the best monitoring in order to reproduce the trend seen by the camera.

- A flag structure containing the above information is generated, as well as a file giving the best monitoring to be applied for each run.

Finally, the quantum efficiency of the detectors and the transmission of the filters is computed using the camera data and beam data structures and the monitoring information derived above.

- The relevant informations are extracted from the beam (e.g. absolute beam profile,) and camera data structures (e.g. mask values, relative positions of the CCDs, counts and number of frames, ...)

- For each camera run, we compare the shape of the horizontal profile as seen by the camera and that of the absolute beam profile measurement (see Fig. 9). The compared profiles are not corrected from monitoring at this stage, since profiles are assumed short enough in time so that their spatial shape should not be affected. On the other hand, both profiles are arbitrarily divided by their median value in order to allow horizontal correlation.

  It appeared that the offset between the horizontal axis of the absolute detector and that of the camera was changing with time, probably because of the repositioning of the camera after each run. We therefore used offsets computed from a maximum correlation between the 2 profiles, rather than that derived from the comb measurements.

  In addition to the offset, a stretch (also varying with time) of the horizontal axis clearly improves the match between the two profiles. This is probably due to a bad reproductibility of the rotation mechanism (after switching beam line) or to some divergence in the beam line (after changing energy, i.e. new monochromator/mirrors settings).

  In some cases, the derived offsets and stretch values computed automatically are too large and not real (problem of computing best correlation between 2 very flat profiles). Such values (above a given threshold) were replaced by the median offset and stretch values associated to runs taken just before and after the considered run. The offsets and threshold used are shown on Fig. 8.

- For each run corresponding to an OPEN position of the camera filter wheel, the QE of all CCDs of the camera are computed using Eq. 3 (see Sec. 4).

- QE values at this stage were also computed for camera measurements obtained through filters, as well as for camera runs with no absolute measurement of the beam intensity (using a dummy value for the absolute value), so that filters transmissions can later be obtained by dividing those fake QE values.

3.2 Data selection strategy

The MOS2 calibration campaign started without chopper attenuator device; metallic filters (on SACO) and grids (on DCI) were used instead to reduce the beam flux. In these cases,

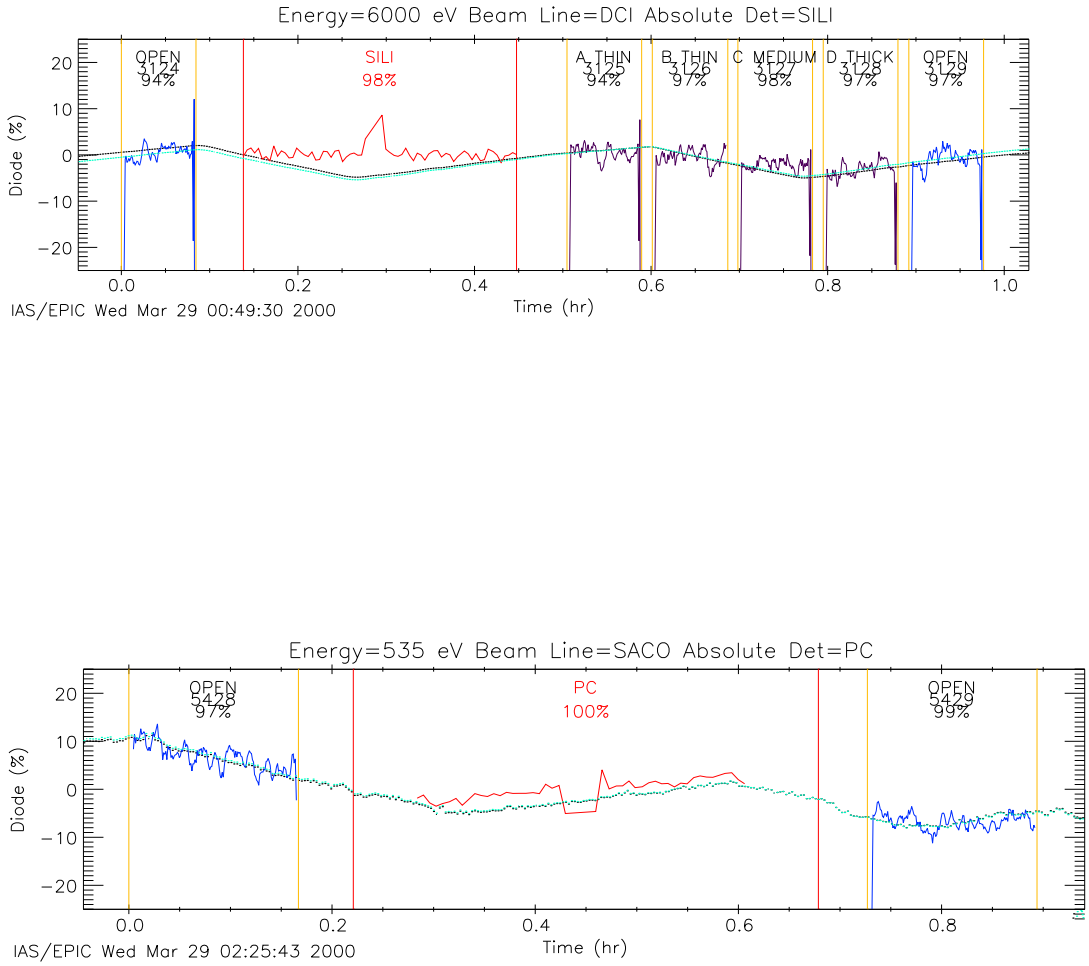

Figure 7: Examples of monitoring plot. Dark Blue: camera data during OPEN measurements, Black: monochromator monitoring signal, Light Blue: monochromator monitoring signal corrected for a linear trend. The vertical bars indicate begining and end of each run.

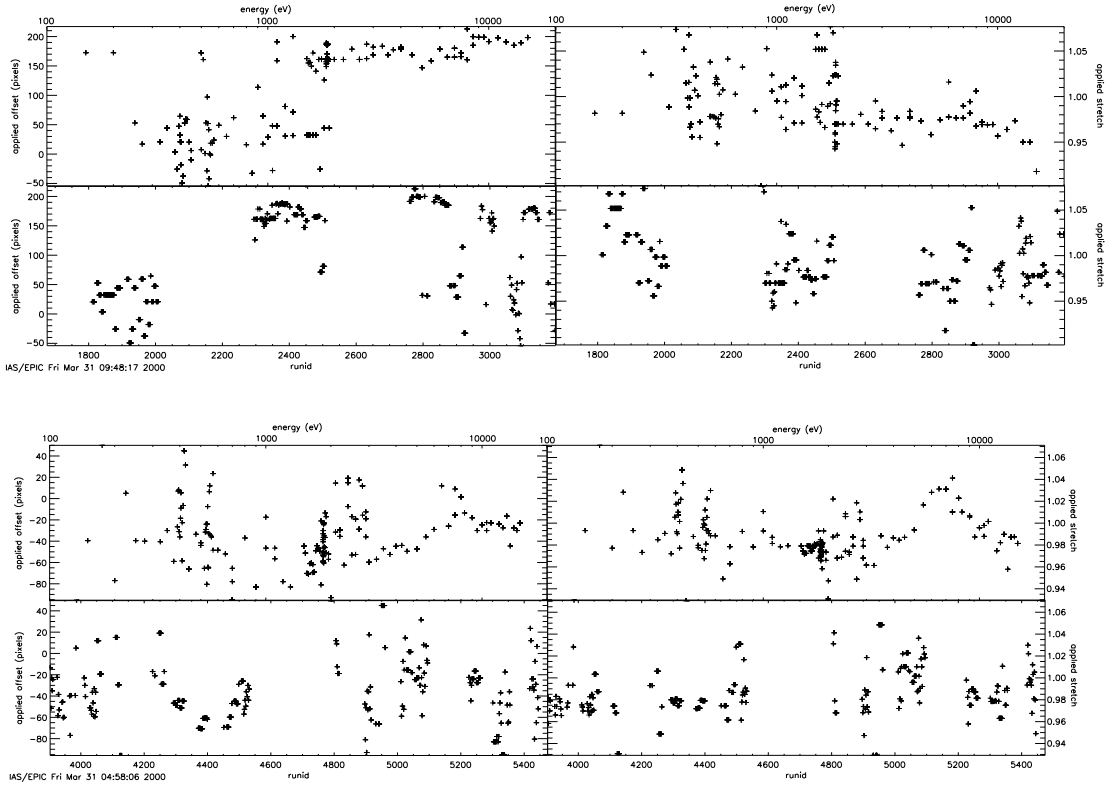

Figure 8: Offset and stretch used for MOS2 (top) and MOS3 (bottom).

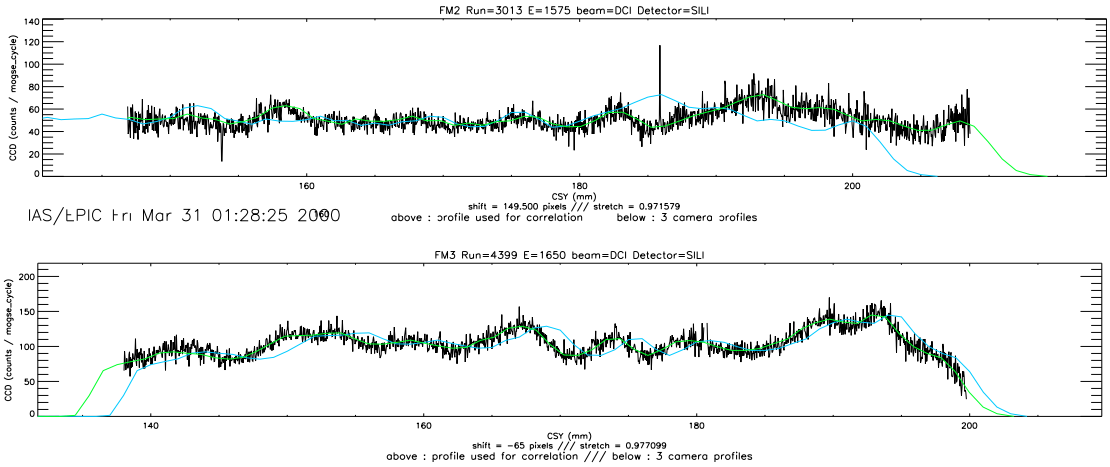

Figure 9: Examples of profile comparison. Dark: camera profile, Blue: profile observed by the absolute detector, Green: offseted and stretched absolute profile.

the absolute profile measurement was done twice, with and without the filter/grid. A direct comparison of both absolute profiles gives the attenuation factor of the filter/grid at the given energy, then the QE calculation procedure is resumed normally (as with the chopper).

A total of 719 logged runs were available for MOS2 processing, including 305 OPEN-filter runs with relevant absolute measurement, on 113 different energies. Of those, 51 runs were rejected (5 because of bad monitoring, 4 because of bad absolute profile, 2 because of calibration test bench misconfiguration, 8 because of bad camera data, 16 because of camera misconfiguration -"threshold mode" instead of "imagery mode"-, 16 because of monitoring and attenuator problems the first day on DCI line), leading to a QE-useful dataset of 254 runs, on 105 different energies.

It is to be noted that among runs performed without chopper, 11 runs missed the attenuation measurement at 395, 400 and 402 eV. The attenuation was then a posteriori assumed after interpolation on other measurement done with the SACO filter, between 200 and 500 eV (see Fig. 10). The resulting QE values derived from those runs fit very well with the remaining MOS2 points.

On a global point a view, the analysis of MOS3 calibration campaign was neither easy nor difficult... It was above all the first to be analysed ! This choice comes from the assumption that calibration runs would be cleaner than for any other MOS campaign, but classical problems (misalignments, monitoring jumps, etc.) would appear anyway in order to design analysis software smart enough to treat them properly.

A total of 682 logged runs were available for MOS3 processing, including 341 OPEN-filter runs with relevant absolute measurement, on 123 different energies. Of those, 26 runs were rejected (6 because of bad monitoring, 2 because of bad absolute profile, 12 because of bad camera data, 6 because of calibration test bench misconfiguration), leading to a QE-useful dataset of 315 runs, on 120 different energies.

4 Quantum Efficiency calculations

Let $< \phi >$ be the average beam flux (phot/s/mm^2) at a given energy E, the total number of counts on a given CCD of the camera will be

$$Counts_{ccd} = QE_{ccd} < \phi > tint_{ccd} N_f S_{ccd} T_{chop} \quad (1)$$

where QE_{ccd} is the average quantum efficiency of the given CCD at energy E, $tint_{ccd}$ is the integration time for one slew of the camera behind the resizing device, N_f is the number of slews (called number of MOGSE frames),T_{chop} is the transmission of the chopper and S_{ccd} is the CCD illuminated surface ($S_{ccd} = N_{Vpix} N_{Hpix} L_{pix}^2 Mask_{ccd}$). The integration time is defined by the vertical size of the resizing device (h) and the velocity of the MOGSE (v) through $tint_{ccd} = h/v$.

The integral of the absolute beam profile over the horizontal region corresponding to the given CCD satisfies

$$\int_{ccd} \frac{Counts_{abs}(CSY)}{L_{abs}\, tint_{abs}\, QE_{abs}} dCSY =< \phi > h\, L_{pix}\, N_{Hpix} \quad (2)$$

where L_{abs} is the absolute detector size along the horizontal axis, $tint_{abs}$ is the integration time and QE_{abs} is the absolute quantum efficiency at energy E. Note that the chopper was inserted in the beam for the camera data taking only.

The average quantum efficiency of the given CCD therefore writes

$$QE_{ccd} = \frac{Counts_{ccd}}{\int_{ccd} Counts_{abs}(CSY) * Mask_{ccd}(CSY)\, dCSY} * \frac{QE_{abs}\, v\, L_{abs}\, tint_{abs}}{N_f\, N_{Vpix}\, L_{pix}\, T_{chop}} * cor_{MO} \quad (3)$$

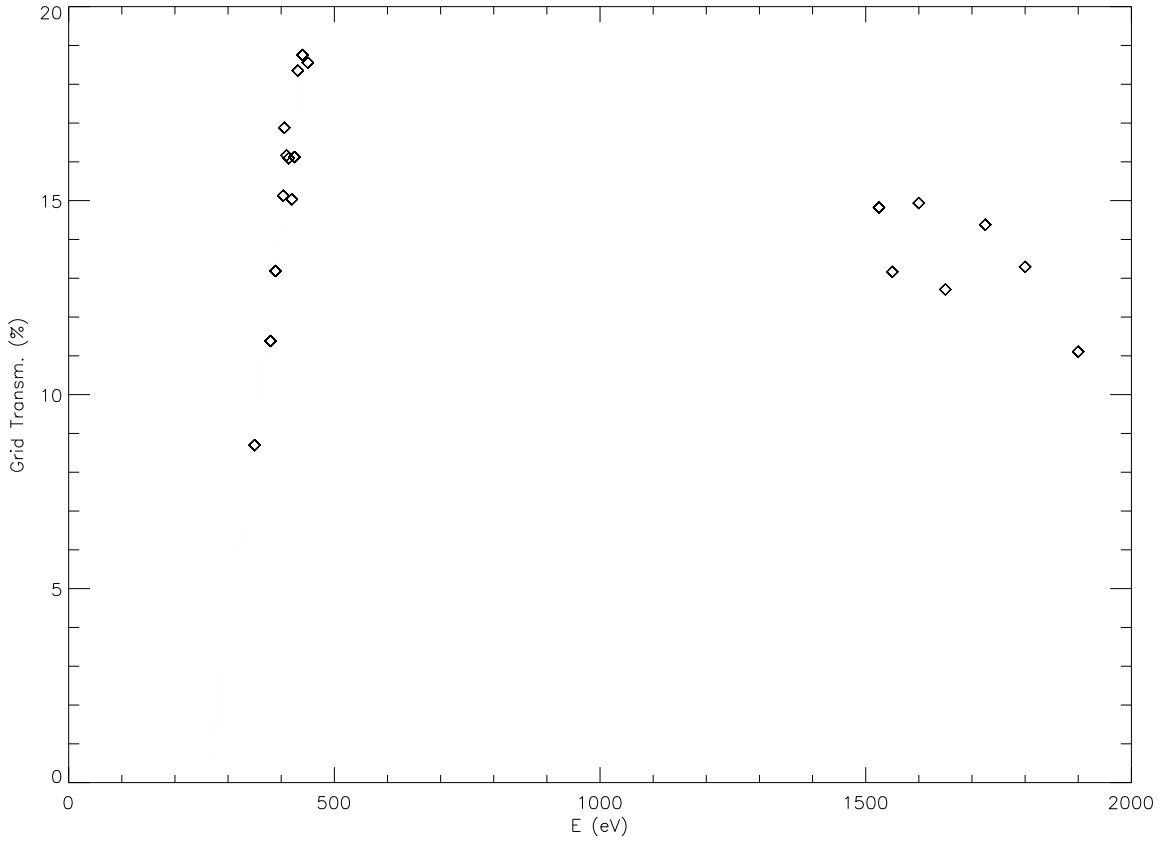

Figure 10: Attenuation of the filter (200-500 eV) and of the grid (above 1.4 keV) with energy. Plain line shows the best linear fit to the filter attenuation (used for interpolation).

Table 1: Constant parameters used to compute QE.

Parameter	value
L_{SiLi}	1.0 mm
L_{PC}	0.1 mm
N_{Vpix}	200
L_{pix}	150 μm
v	24.7 mm/s
T_{chop}	4.6%

where $Mask_{ccd}(CSY)$ is the camera mask (due to obscuration by the circular baffle and bad pixels removal) summed along the vertical axis, and cor_{MO} is a correction factor accounting for the change in beam intensity between the absolute and camera measurements, computed using our best monitoring (see Sec. 3).

The QE values have been computed using the values for the constant parameters entering Eq. 3 given in Tab. 1. The integral of the absolute profile in Eq. 3 is performed over the CSY region corresponding to the given CCD, as derived from the best correlation between camera and absolute horizontal profiles described in Sec. 3. It must be noted that for the vast majority of the runs, the best monitoring was found to come from the monochromator diode.

For the present release, QE values corresponding to the same energy have been averaged, with a weight proportional to the relative error affecting each data point (see Sec. 5). Therefore, a single value of QE is quoted per energy. The final error quoted includes the resulting relative error and the absolute error linked to the absolute calibration uncertainties (see Sec. 5).

Note that QE values for each CCD column instead of the whole CCD could be derived from the ratio of counts profiles instead of the ratio of total counts.

Also, transmission of the filters could be computed by dividing the QE for a given filter by the average of QE values for the OPEN positions observed during the same run series. This result is not presented in this release since the transmissions curves will first have to be compared/merged with the values derived at CEA-Saclay and the Italian team.

5 Error Budget

Tab. 2 evaluates the uncertainty sources in the determination of the QE given above.

An estimate of the actual uncertainty on the Si(Li) detector absolute calibration is given. It increases at high energy where the determination of the Si(Li) quantum efficiency is based on extrapolations of the Bessy results. The dimensions of the collimator have been precisely measured using the CEA profilometer and are used in the present analysis. We have checked the pile-up level of the Si(Li) detector on several Si(Li) spectra which was always found to be lower than 1%.

The quoted "divergence/alignement" errors were derived from the median values of the relative difference between best-monitoring-corrected absolute horizontal profiles and camera horizontal profiles (Fig. 9). The "monitoring" relative error comes from the difference between best monitoring and camera time-ordered data such as shown in Fig. 7.

The speed of the MOGSE system has been shown to be very stable. However, an uncertainty remains about the exact value of this speed, that could be reduced by deep vertical analysis of camera images (which should allow to estimate the apparent movement of the slit across each CCD).

Finally, the main discrepancy between MOS Orsay3 and MOS Orsay2 QE curves resides in the region around Oxygen Edge (500-600 eV), corresponding to the measurements based on GPC absolute profiles (below 300 eV, the MOS cameras are anyway probably as noisy as the GPC is). The QE points based on Si(Li) profiles are consistent for both cameras. A new GPC-Si(Li) intercalibration experiment has been undertaken to better understand why GPC based QE points are so different from one another.

Table 2: QE budget error

Title	MOS cam	relative/absolute
Absolute Detectors:		
Si(Li) QE	$2\%@0.3-1.5keV$ $5\%@1.5-6.0keV$ $10\% > 6.0keV$	absolute
Collimator	1%	absolute
Pile-Up	$<< 1\%$	absolute
Statistics	$< 1\%$	relative
Beam Knowledge:		
Monitoring	$0.5-3.0\%$	relative
Divergence / Alignment	$0.5-10.0\%$	relative
Chopper Transmission	10%	absolute
MOGSE:		
Speed stability	$<< 1\%$	absolute
Speed value	$\simeq 2\%$ (?)	absolute
EPIC:		
Statistics	$< 2\%$	relative